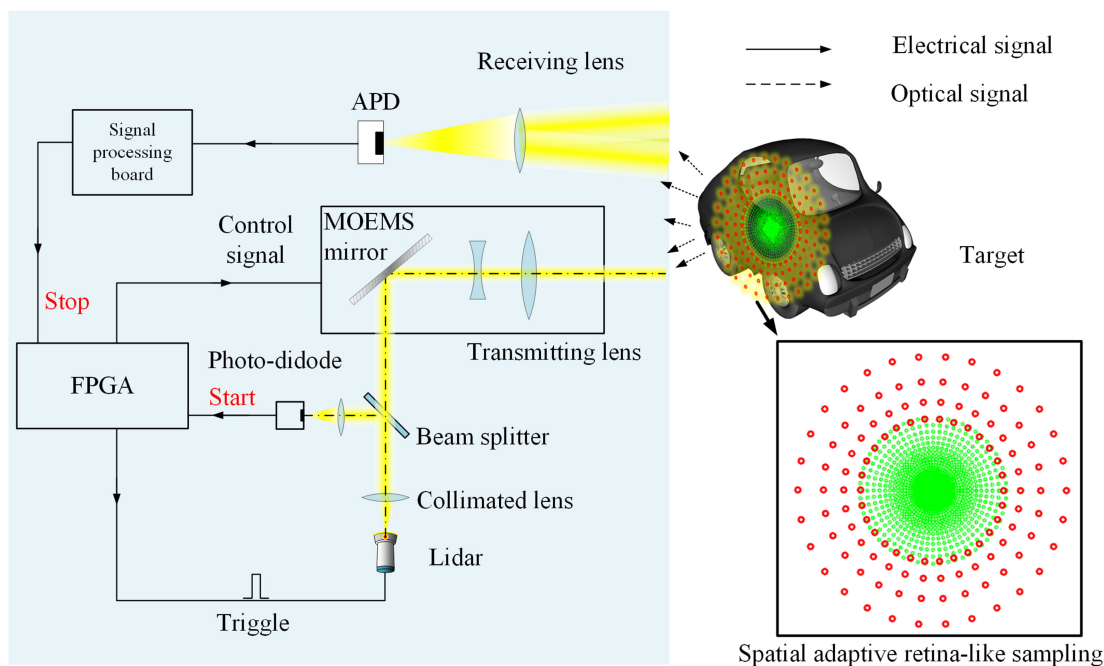



Spatially Adaptive Retina-Like Sampling Method for Imaging LiDAR

Volume 11, Number 3, June 2019

Sihui Li
Jie Cao
Yang Cheng
Lingtong Meng
Wenze Xia
Qun Hao
Yami Fang



Spatially Adaptive Retina-Like Sampling Method for Imaging LiDAR

Sihui Li,¹ Jie Cao ,¹ Yang Cheng,¹ Lingtong Meng,¹ Wenze Xia,¹ Qun Hao,¹ and Yami Fang²

¹Key Laboratory of Biomimetic Robots and Systems, Ministry of Education, Beijing Institute of Technology, Beijing 100081, China

²Shanghai Aerospace Control Technology Institute, Shanghai 201109, China

DOI:10.1109/JPHOT.2019.2910866

1943-0655 © 2019 IEEE. Translations and content mining are permitted for academic research only.

Personal use is also permitted, but republication/redistribution requires IEEE permission.

See http://www.ieee.org/publications_standards/publications/rights/index.html for more information.

Manuscript received March 7, 2019; accepted April 9, 2019. Date of publication April 16, 2019; date of current version May 1, 2019. Corresponding author: Jie Cao (e-mail: ajieanyyn@163.com).

Abstract: To mitigate the conflict between imaging quality and speed, a spatially adaptive retina-like sampling method for 3-D imaging Lidar based on time-of-flight method is proposed. The differences between previous retina-like sampling method and the proposed method are described. Sampling points with dense distribution is for the area of interest while sparse distribution is for the area of uninterest, which obtains high imaging quality while consuming much less data acquisition time. Mathematical models of the spatially adaptive retina-like method are developed, and the key parameters are analyzed. To validate the spatially adaptive retina-like sampling method, we perform situational simulations to compare the proposed method with the previous one. Results demonstrate that the proposed method is capable of decreasing data acquisition time without considerable distortion of the interested target. Furthermore, the proposed method is analyzed under different scenes for single and multiple targets. Results illustrate that the proposed method performs better than the previous method.

Index Terms: Spatially adaptive, retina-like, three-dimensional imaging, LiDAR.

1. Introduction

Light detection and ranging (LiDAR) sensors have attracted much attention in past decades due to their simplicity in principle, ability of anti-interference, and long imaging distance. LiDAR sensors are widely used in various fields, such as mapping, robotics, security, unmanned aerial vehicles, and environment-sensing applications [1]–[7]. According to the type of imaging, these sensors can be divided into scanning and non-scanning types [8], [9]. For the scanning type, different scanners (e.g., MEMS mirror, galvanometer scanner) have been employed in the imaging LiDAR to obtain images with a large field of view (FOV) and high resolution [10], [11]. However, the information of target is obtained by point-by-point sampling through scanners. Thus, this type of LiDAR suffers from large time consumption and low efficiency, which restrict its real-time applications. Different from the scanning type, the non-scanning type uses avalanche photo diode (APD) array instead of scanners to sample the information of the target [12], [13]. The resolution of this type largely relies on the pixel number of the APD array [9]. However, an APD array with a large pixel number (larger than 64×64) is difficult to obtain due to limited APD fabrication technology and crosstalk noise. To obtain a high-resolution image, the scanning-type imaging LiDAR remains an available choice, but at the cost of large time consumption and low imaging efficiency.

Many methods have been devoted to improving imaging efficiency while maintaining the high resolution of the scanning-type sensor. Markus Henriksson *et al.* introduced a single pixel time-correlated single-photon-counting LiDAR system [14]. One row of the scene is collected for each sweep during the measurement in this system, and this reduces the overhead associated with the scanning, compared with point-by-point scanning, thereby allowing the measurement of large scenes simultaneously. Ling Ye *et al.* proposed a spatially adaptive imaging method for LiDAR by exploiting discontinuities between target and background in the depth domain to localize the areas near the depth boundaries and perform fine scanning only to these areas, and this ensures recovery accuracy and short data acquisition time [15].

Our group previously proposed a retina-like scanning method based on MEMS mirror to improve the imaging efficiency for the scanning type of LiDAR [16]. The image obtained by the retina-like sampling method has a variable spatial resolution, which possesses high resolution in the center and low resolution in the periphery of the FOV. Moreover, the relationship between the retina and the visual cortex is subject to an approximate logarithmic-polar law, which is beneficial to compress redundant data. These properties of the retina-like scanning method can improve imaging efficiency. However, using retina-like sampling with the same decreasing coefficient of the entire spatial area is not necessary when the area of interest only occupies a portion of the whole FOV. More effective sampling points on the interested target and less sampling points on the area of uninterest can further increase imaging efficiency. Therefore, we propose a spatially adaptive retina-like sampling method by sampling the data of interest with a small decreasing coefficient and the area of uninterest with a large decreasing coefficient. Compared with our previous retina-like scanning method, the proposed method not only can further compress redundant data in the area of uninterest, but also provide a higher resolution in the area of interest. It balances the relationship between high resolution and high efficiency for the scanning type of LiDAR.

The rest of the paper is organized as follows: The working principle of the proposed sampling method is introduced in Section 2; the mathematical model of the retina-like sampling and the key processes of the proposed method are illustrated in this section. Then, in Section 3, we compare the results obtained by the proposed method and previous retina-like sampling method under different proportions of the target's and the FOV's size. Furthermore, comparison of the proposed method and the previous retina-like sampling method under multi-object imaging scene is conducted. We also discuss the effect of different values of depth threshold (τ) and difference threshold (σ) on spatially adaptive retina-like imaging LiDAR in Section 4. Finally, conclusions and future studies are listed in the last section.

2. Methods and Material

2.1 Principle

The principle of LiDAR based on spatially adaptive retina-like sampling method is shown in Fig. 1. First, a pulsed laser is triggered by an FPGA and output a pulsed laser beam. Second, the pulsed laser beam is divided into two beams by a beam splitter. One beam is focused on a photodiode by a focusing lens, and the output signal of the photodiode is regarded as the start moment for the timer in the FPGA. Another beam is collimated and projected to the object scene via a transmitting lens. The object surface is scanned by the beam spot using the spatially adaptive retina-like sampling method, which is controlled by a micro-opto-electro-mechanical-system component. A detailed description of the spatially adaptive retina-like sampling method is presented in Section 2.2. Third, the reflected or scattered pulsed echo from the object is focused on the APD detector through a receiving lens. Lastly, the signal generated by the APD detector is filtered and amplified by a signal processing board, and the processed signal is regarded as the stop moment for the timer. The distance between the object surface and the pulsed laser can be obtained according to the time interval between the stop moment and the start moment, i.e., the time-of-flight (TOF). Retina-like scanning has the intrinsic property from Cartesian coordinates to log-polar coordinates; thus, the log-polar image of the object can be obtained directly via retina-like scanning [16]. Therefore, the

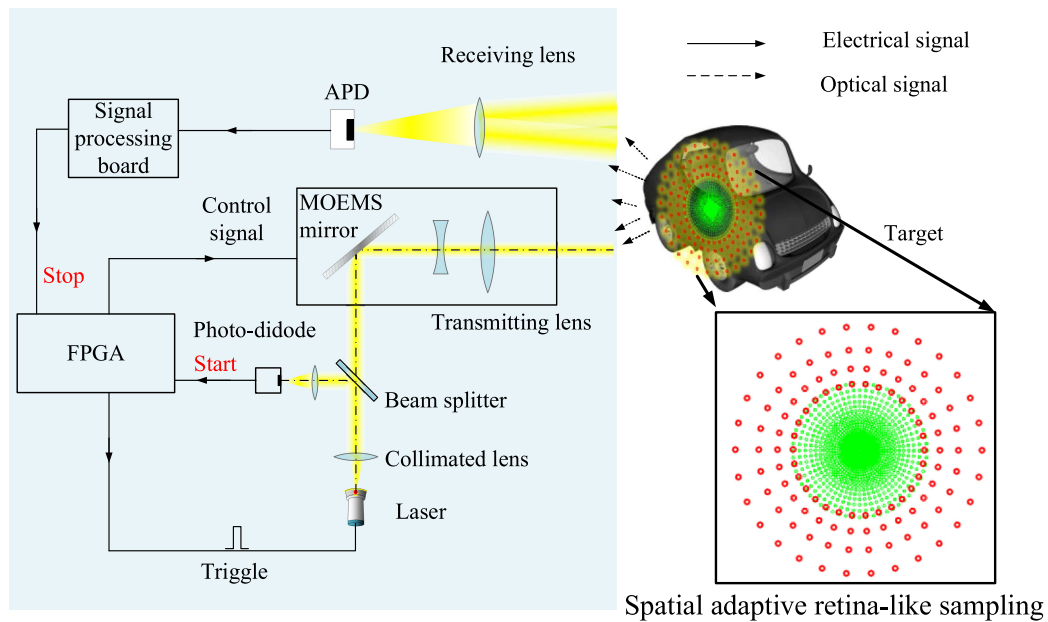


Fig. 1. Principle of the Lidar based on spatially adaptive retina-like sampling method.

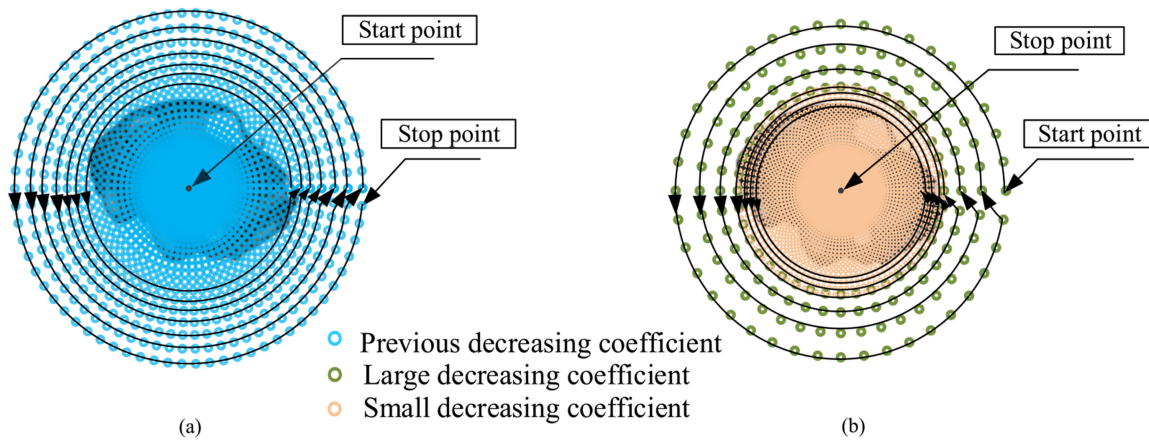


Fig. 2. Comparison of two retina-like sampling methods. (a) Previous retina-like sampling. (b) Spatially adaptive retina-like sampling.

peripheral redundant data is compressed, while high-resolution imaging is performed on the central area.

2.2 Comparison of the Proposed Method and Previous Method

To illustrate the difference between the previous retina-like sampling method and the proposed method clearly, two scanning types are shown in Fig. 2. On the one hand, the scanning track of the previous retina-like sampling method starts from the innermost ring and ends with the outermost ring. By contrast, the proposed method starts from the outermost ring and ends with the innermost ring for profile estimation of the object with fewer scanning points. On the other hand, the previous retina-like sampling method scans the entire object scene with the same decreasing coefficient. However, scanning the area of uninterest with the same decreasing coefficient as the area of

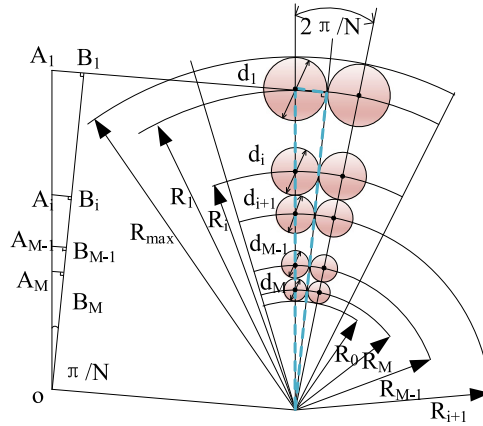


Fig. 3. Mathematical model of retina-like sampling.

interest is not necessary, when the area of interest only occupies a portion of the whole FOV. Therefore, unlike the previous retina-like sampling method, the proposed method performs retina-like sampling with a different decreasing coefficient in the object scene. A retina-like sampling with a small decreasing coefficient is performed on the area of interest, and a large decreasing coefficient sampling is performed on the area of uninterest. Thus, the object scene is adaptively divided into low- resolution and high-resolution imaging areas. The proposed sampling method provides rich imaging details for the area of interest and low information on the outside area of the area of interest, resulting in the mitigation of the conflict between imaging accuracy and imaging speed.

2.3 Mathematical Modeling of the Spatially Adaptive Retina-Like Sampling

According to the model of retina-like sampling, the relationship between the sampling radius of two adjacent rings follows an exponential decreasing law [17]. Usually, the number of rings (M) and sectors for each ring (N), and the radius of the sampling FOV (R_{\max}), are known for the user. R_0 is the radius of the blank area, and R_i is the radius of the i -th sampling ring. d_i is the expected spot diameter of the i -th sampling ring. The location of the sampling point is the central point of the expected spot diameter. The angle between two adjacent sectors is $2\pi/N$, because the two sectors are tangent. A_i is the center point of the spot of the i -th sampling ring, and B_i is the corresponding tangency point. According to the geometric relationship in Fig. 3, we can obtain $\angle A_M O B_M = \pi/N$, $OA_M = R_M$, $A_M B_M = R_M - R_0$. The derivation of the decreasing coefficient meets the following equation:

$$\begin{cases} \frac{d_i}{2} = R_i \times \sin(\pi/N) \\ \frac{d_{i+1}}{2} = R_{i+1} \times \sin(\pi/N) \\ R_{i+1} = R_i - \frac{d_i}{2} - \frac{d_{i+1}}{2}, R_{i+1} = R_i \cdot q \end{cases} \Rightarrow q = \frac{1 - \sin(\pi/N)}{1 + \sin(\pi/N)} \quad (1)$$

From Eq. (1), we find that the value of q is less than 1, because the scanning track starts from the outermost ring with a large radius and ends with the innermost ring with a small radius. $1/q$ is defined as the decreasing coefficient. The radius of each ring should be subject to the following exponential relationship:

$$R_i = R_1 \cdot q^{i-1}. \quad (2)$$

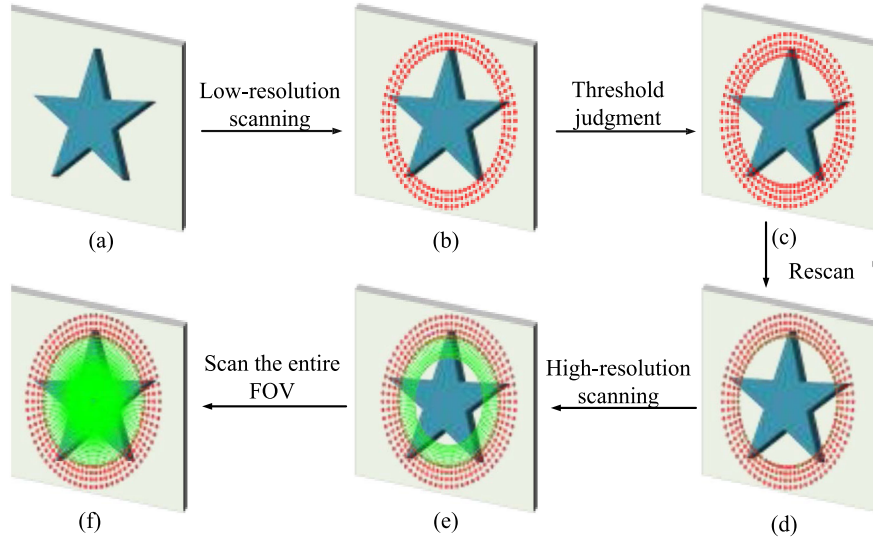


Fig. 4. Flow chart of our method. (a) Image scene. (b) Scanning under a large decreasing coefficient. (c) Retina-like sampling under a large decreasing coefficient is completed. (d) Retina-like sampling begins with a small decreasing coefficient. (e) Scanning under a small decreasing coefficient. (f) Retina-like sampling under a small decreasing coefficient is completed.

Moreover, according to the theory analysis based on the structure feature of the human retina, the derivation of the relationship between R_{\max} , R_0 , M , and N is as follows:

$$\begin{cases} R_0 = R_M \times [1 - \sin(\pi/N)] \\ R_1 = \frac{R_{\max}}{1 + \sin(\pi/N)} \\ R_i = R_1 \cdot q^{i-1} \end{cases} \Rightarrow R_0 = R_{\max} \cdot q^M \quad (3)$$

Unlike the previous retina-like sampling method, the proposed method consists of two retina-like sampling models with different decreasing coefficients. Here, we use a simple scene (Fig. 4(a)) to illustrate the steps of a spatially adaptive retina-like sampling method. The scene contains a flat and a board, which means that two range values are present in the depth image, as shown in Fig. 4(a).

The parameters of the first model of retina-like sampling are $R_{\max 1}$, M_1 , and N_1 . The scanning track starts from the outermost ring with the radius $R_{\max 1}$ under a large decreasing coefficient, as shown in Fig. 4(b). The depth value of the scanning point at the j -th sector of the i -th ring is measured by the TOF method and is defined as $P_{i,j}$. The process of the first model of retina-like sampling is completed until Eq. (4) is satisfied (Fig. 4(c)).

$$\begin{cases} f(x) = \begin{cases} 1 & |x| < \tau \\ 0 & |x| \geq \tau \end{cases} \\ D_i = \sum_{j=1}^{N_1} f(P_{i,j} - P_{i,j+1}) + f(P_{i,j} - P_{i-1,j}) \geq \sigma, \text{ where, } P_{i,N_1+1} = P_{i,1} \end{cases} \quad (4)$$

where D_i is the sum of the number of sampled object point distinguished from background point in the i -th ring; and τ and σ are the thresholds determined by the actual situation. The manner of selection of the values of τ and σ is discussed in Section 4. The process of the second model of retina-like sampling starts from the i -th ring with the parameters of $R_{\max 2}$, M_2 , and N_2 ($N_2 > N_1$), where $R_{\max 2} = R_i$, and M_2 and N_2 are set according to actual needs; the second model sampling start is shown in Fig. 4(d). The decreasing coefficient of the second model of retina-like sampling obtained by Eq. (1) is smaller than that of the first model. Therefore, the image sampled by the second model has a higher resolution, as shown in Fig. 4(e). The left sampling processes is

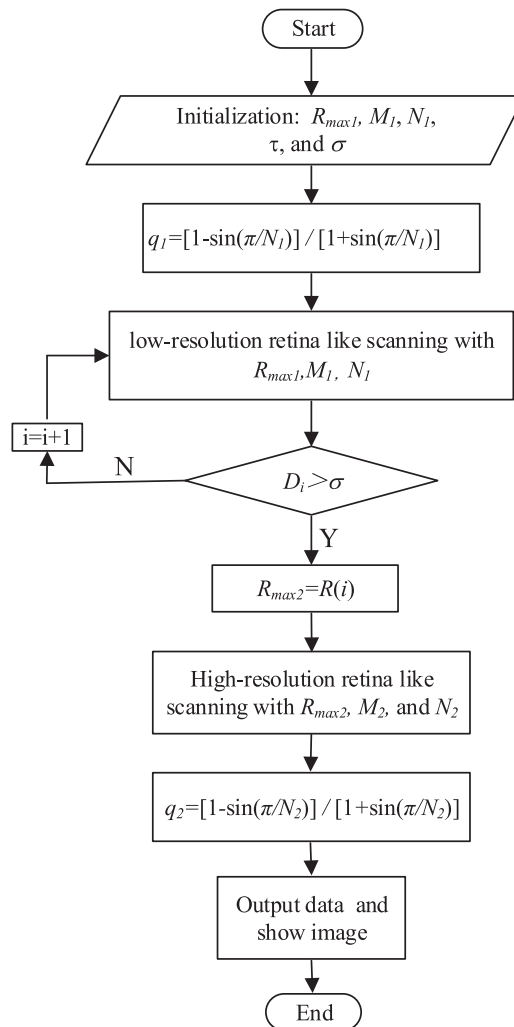


Fig. 5. Workflow of the spatially adaptive retina-like sampling method.

completed by the second model in Fig. 4(f). The workflow describing the aforementioned process is represented in Fig. 5.

3. Results and Simulation

3.1 Modeling Verification

To verify the validity of the spatially adaptive retina-like sampling method for balancing the imaging efficiency and imaging resolution, a tank model downloaded from the Princeton Shape Benchmark [18], whose size is $7 \times 3.5 \times 2.8$ m³ (L \times W \times H) is taken as an example (shown in Fig. 6(a)). We set typical parameters in the following simulation to compare these two scanning methods (previous retina-like scanning and spatially adaptive retina-like scanning). The simulation parameters are shown in Table 1.

We suppose that the interested area of target is located on the center of FOV. Γ_{TF} is defined as the proportion of the largest dimensional size of the target's three sizes and the larger dimensional size of the FOV's two sizes. A depth image with 366×500 sampling points (rings \times sectors)

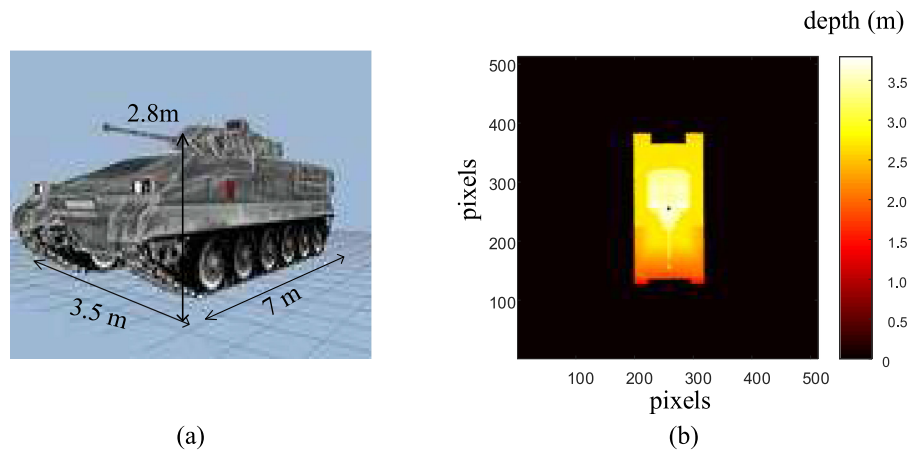
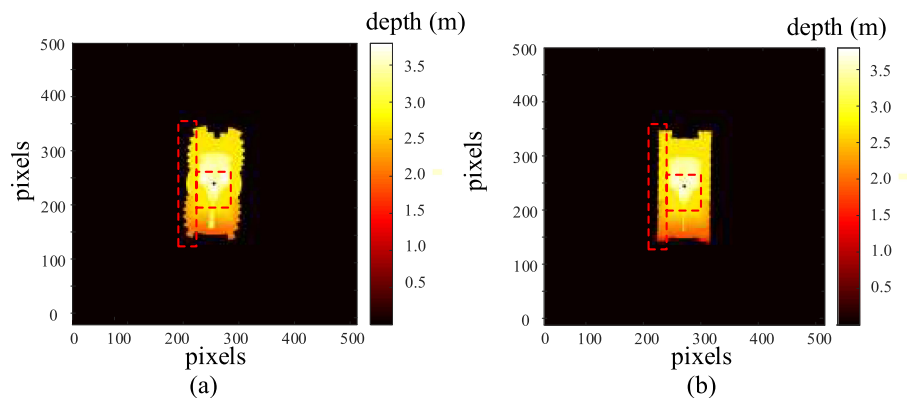


Fig. 6. Tank model and reference image.

TABLE 1
Parameter Values Used in the Simulation

Method	Rings	Sectors
Retina-like scanning (Reference image)	$M_R=366$	$N_R=500$
Previous retina-like scanning with low resolution	$M_{TL}=36$	$N_{TL}=50$
Previous retina-like scanning with high resolution	$M_{TH}=146$	$N_{TH}=200$
Spatially adaptive retina-like scanning in background area	$M_1 \in (1-36)$	$N_1=50$
Spatially adaptive retina-like scanning in tank area	$M_2 \in (0-146)$	$N_2=200$

Fig. 7. Two depth images obtained by the previous retina-like sampling method. (a) Low-resolution with 36×50 pixels. (b) High-resolution with 146×200 pixels.

using the previous retina-like sampling method is considered as the reference image, as shown in Fig. 6(b). The target occupies about 40% of the field size, i.e., $\Gamma_{TF} = 40\%$.

Two depth images with different resolutions obtained by the previous retina-like sampling method are shown in Fig. 7(a) shows the depth image with low resolution at 36×50 sampling points (rings \times sectors), and Fig. 7(b) shows the depth image with high resolution at 146×200 sampling (rings \times sectors). Compared with Fig. 7(a), the image in the periphery of the FOV is distorted due to

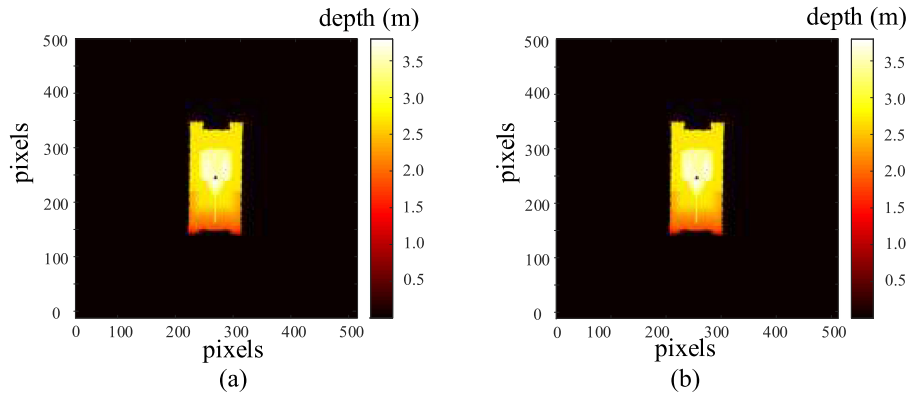


Fig. 8. (a) Depth image obtained by the previous retina-like sampling method with 146×200 pixels. (b) Depth image obtained by the proposed retina-like sampling method.

the small number of sampling points in Fig. 7(b), and some detailed information are missing near the turret of the tank, as shown in the red dashed rectangle in Fig. 7. This phenomenon can be alleviated by increasing the number of sampling points based on the previous retina-like sampling method, as shown in Fig. 7(b).

However, from Fig. 7(b), many sampling points can be observed beyond the tank model, because the background information and the tank model information are sampled with the same decreasing coefficient, which results in the decrease in imaging efficiency. Therefore, to compress the background information further and increase the target information, a spatially adaptive retina-like sampling with different decreasing coefficients is performed. The decreasing coefficient of the sampling on the background area equals to that in Fig. 7(a), i.e., $q_1 = 0.8818$, and that on the tank area equals to that in Fig. 7(b), i.e., $q_2 = 0.9691$. The results obtained by both sampling methods are shown in Fig. 8(a) and (b). Image sampling by the proposed method has the approximate resolution on the tank area. However, the number of sampling points by the proposed method is 24,700 ($6 \times 50 + 122 \times 200$), which provides a 15% reduction (i.e., $[1 - (24700/29200) \times 100\%]$) of the sampling points compared with that in Fig. 8(a) (Fig. 7(b)). Therefore, the proposed method is capable of increasing imaging efficiency.

3.2 Results

3.2.1 Comparison of Single Target Imaging With Different Γ_{TF} : To quantify the advantage of the proposed method, a structured similarity (SSIM) [19], [20] is used to evaluate the level of similarity between the image produced by the previous method as well as the proposed method and the reference image, as shown in Fig. 6(b). Ideally, SSIM is equal to one, which means that the output image is similar to the reference image. The larger the value of the SSIM, the more similar the output image is to the reference image [19]. The proportion of the target's size and the FOV's sizes varies in many cases (i.e., the value of the Γ_{TF}); thus, adjusting the parameters of the spatially adaptive retina-like sampling model is necessary. Results of the proposed method are compared with the previous retina-like sampling method under a different Γ_{TF} to test the validity of the proposed method. To ensure that the two methods have the same FOV, the same maximum radius of FOV (i.e., $R_{\max} = R_{\max_1}$) and the same radius of the blank area (R_0) are needed. The parameters of the previous retina-like sampling method are $R_{\max} = 5$, $M = 146$, and $N = 200$. R_0 is 0.05, calculated by Eq. (5). The parameters of the proposed method for low resolution are $R_{\max_1} = 5$, $M_1 = 36$, $N_1 = 50$. R_{\max_2} for the high-resolution area varies according to the modeling of the proposed method described in Section 2.3. The sector number of each ring for the high-resolution area is set

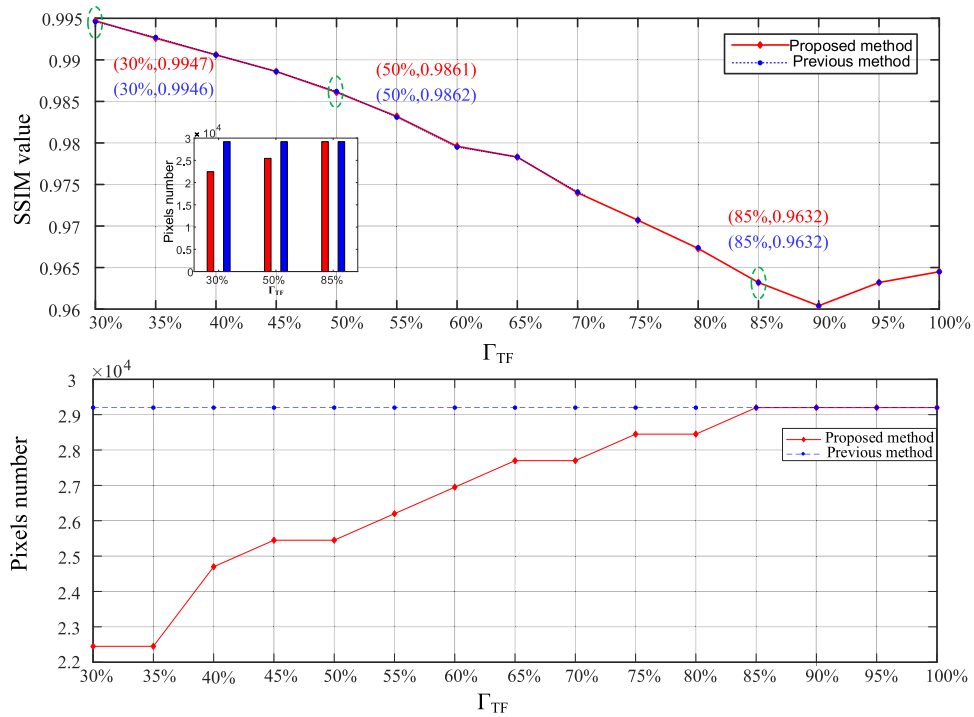


Fig. 9. top: SSIMs of the proposed method and the previous retina-like sampling method under different Γ_{TF} . The red line represents the proposed method, and the blue dashed line represents the previous method. The bar chart on the lower left depicts the number of pixels in the two methods when $\Gamma_{TF} = 30\%$, 50% , and 85% . Bottom: Pixels number of the proposed method and the previous retina-like sampling method under different Γ_{TF} .

to 200, i.e., $N_2 = 200$. The value of M_2 is changed by the following equation:

$$\begin{cases} R_0 = R_{\max 2} \cdot q_2^{M_2} \\ q_2 = \frac{1 - \sin(\pi/N_2)}{1 + \sin(\pi/N_2)} \end{cases} \Rightarrow M_2 = \log_{q_2} \frac{R_0}{R_{\max 2}}. \quad (5)$$

The SSIMs of the proposed method and the previous retina-like sampling method under different Γ_{TF} (from 30% to 100%) are shown in the top of Fig. 9. The red line and the blue line represent the SSIMs of the proposed method and the previous retina-like sampling method, respectively.

The retina-like sampling possesses the characteristics of dense sampling in the central area and sparse sampling in the peripheral area. Thus, the SSIMs of both methods decrease with the increase in Γ_{TF} . It demonstrates that the retina-like sampling performs better when the Γ_{TF} is smaller. However, the value of Γ_{TF} should not be too small in practical situations, because considering whether the distance interval between two adjacent sampling points is sufficient is necessary to distinguish two laser spots. To illustrate the advantages of the proposed method clearly, the pixels number under different values of Γ_{TF} are compared in the bottom of Fig. 9. Fig. 10 shows the sampled images of the two sampling methods under different values of Γ_{TF} .

Pixel number of the proposed method increases with the increase of the values of Γ_{TF} , while the number of pixels in the previous method remains the same ($146 \times 200 = 29200$). When the Γ_{TF} is 30%, the SSIMs obtained by the proposed method and the previous retina-like sampling method are 0.9947 and 0.9946, respectively. The SSIM difference values between these two methods is 0.0001, which indicates that the image sampled by these two methods has approximately the same imaging quality. However, the pixels number of the previous retina-like sampling method is 29200, and that of the proposed method is 22450. Results show that the proposed method use 77%

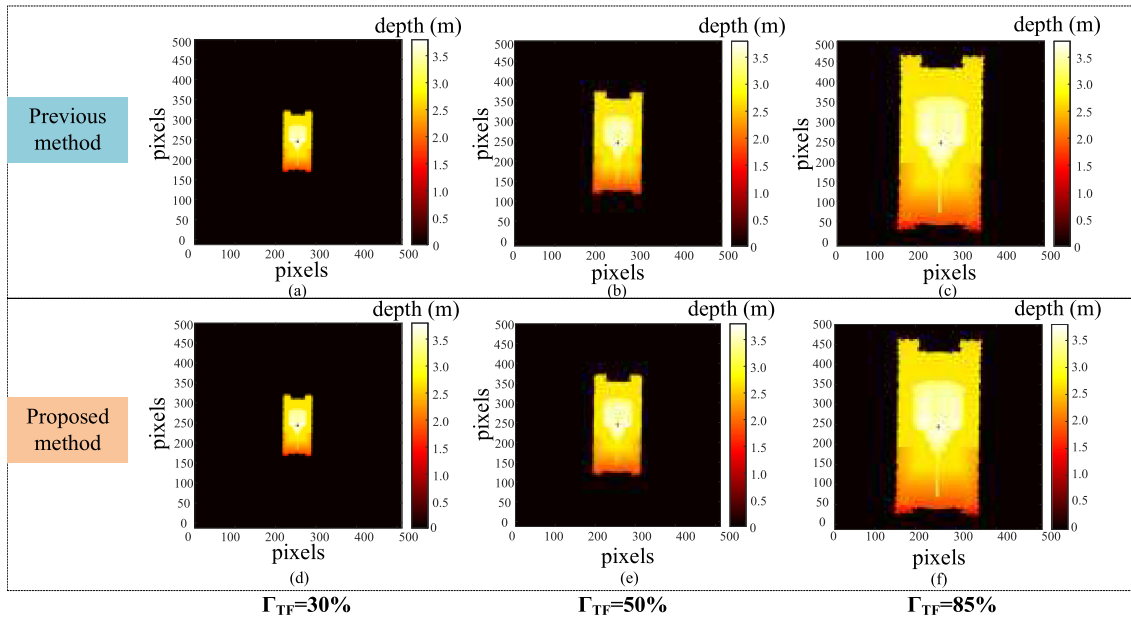


Fig. 10. Sampled images of the proposed method and the previous retina-like sampling method under different values of Γ_{TF} .

[(22450/29200 \times 100%)] times of that by the previous retina-like sampling method and possess approximately the same imaging quality. The same results can be obtained when the Γ_{TF} is 50%. The proposed method uses 87% [(25450/29200 \times 100%)] times of that by the previous retina-like sampling method. However, with the further increase in Γ_{TF} , the pixels number of the proposed method approximately equals to that of the previous retina-like sampling method. When the Γ_{TF} exceeds 85%, the adaptive retina-like imaging results are consistent with the previous method. Therefore, the proposed method shows its superiority when the Γ_{TF} is less than 85% in this case.

3.2.2 Comparison of Multi-Object Imaging: To compare the capability of the spatially adaptive retina-like sampling method with the previous method for balancing the imaging efficiency and the imaging resolution under a imaging scene containing multiple objects, a scene with four objects (a pentagram, a triangle, a rectangle, and a circle) is taken as an example (Fig. 11(a)). Suppose that the pentagram is the interested target, while the other three objects are the uninterested targets. These four objects have different depths from the background, they are 30cm, 15cm, 20cm, 10cm respectively. we choose the depth threshold(25 cm) and difference threshold(3) according to the depth value of objects and prior knowledge. Different from Section 3.2.1, the center of the imaging FOV is not at the center of the interested object. We set the sampling parameters in the following simulation as shown in Table 2.

We compare the proposed adaptive retina-like scanning method with the low-resolution scanning and high-resolution scanning of the previous method to image the multi-targets scene at the same FOV. In Fig. 11(b), The entire FOV is sampled by the previous retina-like scanning method with low-resolution, which uses 12190 pixels(106 \times 115, rings \times sectors) to sample the entire FOV. A spatially adaptive retina-like sampling method with different decreasing coefficients is performed under the same FOV, shown in Fig. 11(c). The areas on both sides of the interested target area are sampled with large decreasing coefficient ($q_1 = 0.9391$, $q_3 = 0.9244$), and the interested target area is sampled with a small decreasing coefficient ($q_2 = 0.9752$). It should be noted that M_1 , M_2 and M_3 are respectively one of the sampling parameters for determining the current regional sampling model, rather than the actual number of sampling rings in each region during the actual sampling process. The actual number of sampling rings is related to the real scene and the threshold. Fig. 11(d) shows the sampling model of previous retina-like scanning method with high-resolution.

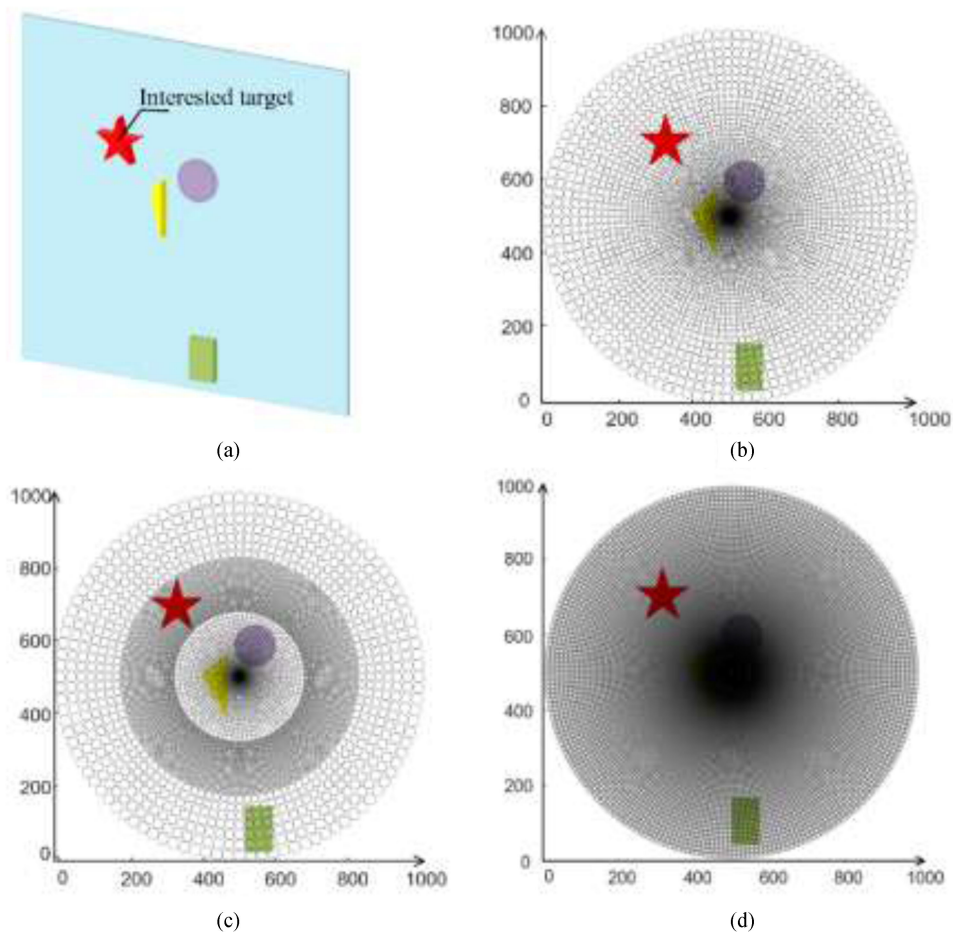


Fig. 11. (a) The imaging scene. (b) The scan pattern of the previous method with low-resolution. (c) The scan pattern of the proposed method. (d) The scan pattern of the previous method with high-resolution.

TABLE 2
Parameter Values Used in the Simulation

Method	Rings	Sectors	q
Previous retina-like scanning with low resolution	$M_L=106$	$N_L=115$	$q_L=0.9468$
Previous retina-like scanning with high resolution	$M_H=230$	$N_H=250$	$q_H=0.9752$
Spatially adaptive retina-like scanning in outer area	$M_1=92$	$N_1=100$	$q_1=0.9391$
Spatially adaptive retina-like scanning in area of interest	$M_2=230$	$N_2=250$	$q_2=0.9752$
Spatially adaptive retina-like scanning in inner area	$M_3=73$	$N_3=80$	$q_3=0.9244$

The value of N_H in this model is equal to the value of N_2 in the adaptive scanning method, ie, $q_H = q_2$. Table 3 shows the total number of pixels sampled for this scene in the three patterns, and Fig. 12 shows the results for the three patterns.

TABLE 3
Pixels Number Used in the Three Cases

Method	Rings	Sectors	pixels
Previous retina-like scanning with low resolution	$M_L=106$	$N_L=115$	12190
Previous retina-like scanning with high resolution	$M_H=230$	$N_H=250$	57500
Spatially adaptive retina-like scanning in outer area	$M_{outer}=7$	$N_{outer}=100$	700
Spatially adaptive retina-like scanning in area of interest	$M_{ring}=24$	$N_{ring}=250$	6000
Spatially adaptive retina-like scanning in inner area	$M_{inner}=61$	$N_{inner}=80$	4880

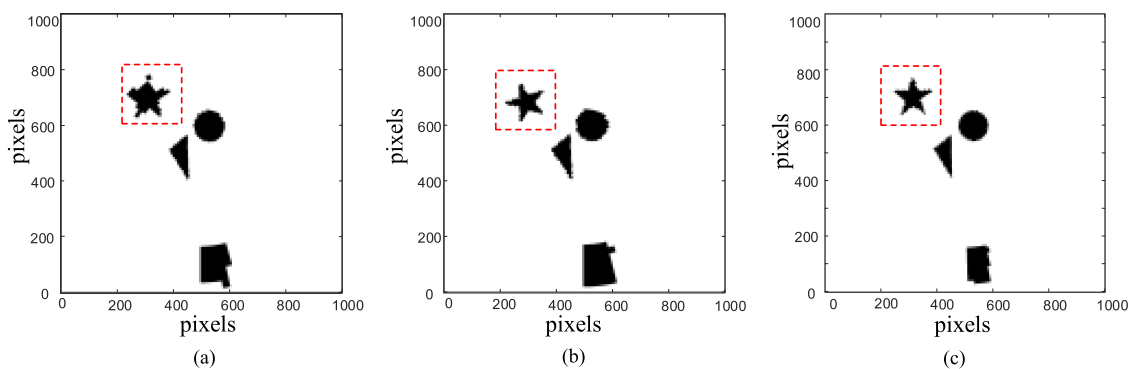


Fig. 12. Results of the two methods: (a) Previous retina-like sampling method. (b) Spatially adaptive retina-like sampling method. (c) Previous retina-like sampling method with high resolution.

Fig. 12(a) is the depth image obtained by the previous retina-like sampling method at 12190 pixels, and Fig. 12(b) is the depth image obtained by the spatially adaptive retina-like sampling method with different decreasing coefficients. The number of pixels in the area of interest is 24×250 (rings \times sectors), and the numbers of pixels in the inner and outer areas are 61×80 and 7×100 , respectively. Therefore, the total number of pixels in Fig. 12(b) ($7 \times 100 + 61 \times 80 + 24 \times 250 = 11580$) is approximately equal to that in Fig. 12(a), which means that they have approximately the same data acquisition time [21], [22]. However, the interested target (pentagram) has a rough imaging edge, and the shape features are not obvious in Fig. 12(a). Compared with Fig. 12(a), the pentagram has a clear outline of geometric features, which indicates that the image quality of the pentagram in Fig. 12(b) is better than that of Fig. 12(a).

For the image with high resolution of the previous method, as shown in Fig. 12(c). It is apparent that all objects in the FOV are imaged with high resolution. In the area where the pentagram is located, current method and the proposed method have the same decreasing coefficient. This means that they have similar resolution for the interested target. However, since the previous method with high-resolution shows dense sampling in the entire FOV, Fig. 12(c) contains 57,500 pixels. It is about 5 times the number of pixels in Fig. 12(b). In summary, the imaging efficiency of the proposed method is greatly improved compared with the previous method with high resolution.

4. Discussion

From the above introduction of method and simulations, discussing the effect of different values of τ and σ on spatially adaptive retina-like imaging Lidar, which directly affects the model of spatially

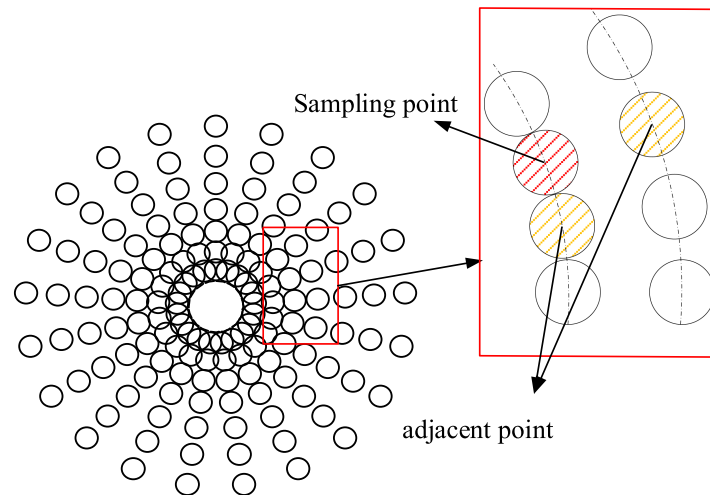


Fig. 13. Sampling and adjacent points in spatially adaptive sampling.

adaptive retina-like sampling and imaging results, is necessary. Based on the scene mentioned in Section 3, the effect of different values of τ and σ on imaging will be discussed.

4.1 Depth Threshold (τ)

According to the analysis of Eq. (4) in Section 2, this parameter is compared with the difference depth value between each point and the adjacent point sequentially, as shown in Fig. 14. If the difference depth value exceeds the threshold τ , D_i is increased by 1. Although the value of τ can be adjusted in real time according to the actual situation, it has a limited condition, which is the range resolution of the Lidar system, i.e., $\tau \geq$ range resolution. Incidentally, based on the principle of TOF, the range resolution is defined as the smallest distance between two targets along the optical axis.

In practical applications, the designer can select a different depth threshold τ , according to the estimation of the degree of difference depth value between the boundary of the target and the background information. For a large value of difference, a relatively large value of τ should be selected. For a small difference, a smaller value of τ should be selected. For the simulation experiments in Section 3, the value of τ is 0.1 m.

4.2 Difference Threshold (σ)

The difference threshold σ is another important parameter to determine the spatially adaptive retina-like sampling model. The dense sampling boundary in the spatially adaptive scanning process is decided by comparing the difference threshold σ with the number of depth difference of each ring (D_i). Dense sampling is started until D_i is greater than σ .

To describe the effect of the value of σ on imaging quality, the SSIM values in the different ranges of σ are shown in Fig. 15(a). Fig. 15(b)–(g) are the imaging results of the target (left) and the corresponding scanning trajectory (right) in the different ranges of σ , respectively. The value of Γ_{TF} is 50%, and the other parameters of this scene are the same with the simulation mentioned in Section 3.

Fig. 15(a) shows that the SSIM of the image gradually decreases during the change of σ from 0 to 100, because the increase of the σ causes the boundary of the dense sampling area to be closer to the center. That is, the dense sampling area becomes smaller with the increase in σ , as shown in Fig. 15(b)–(g). Comparing the imaging results suggests that a dense sampling area will obtain abundant imaging details. If the designer wants a more detailed target information in practice, the σ should be set smaller.

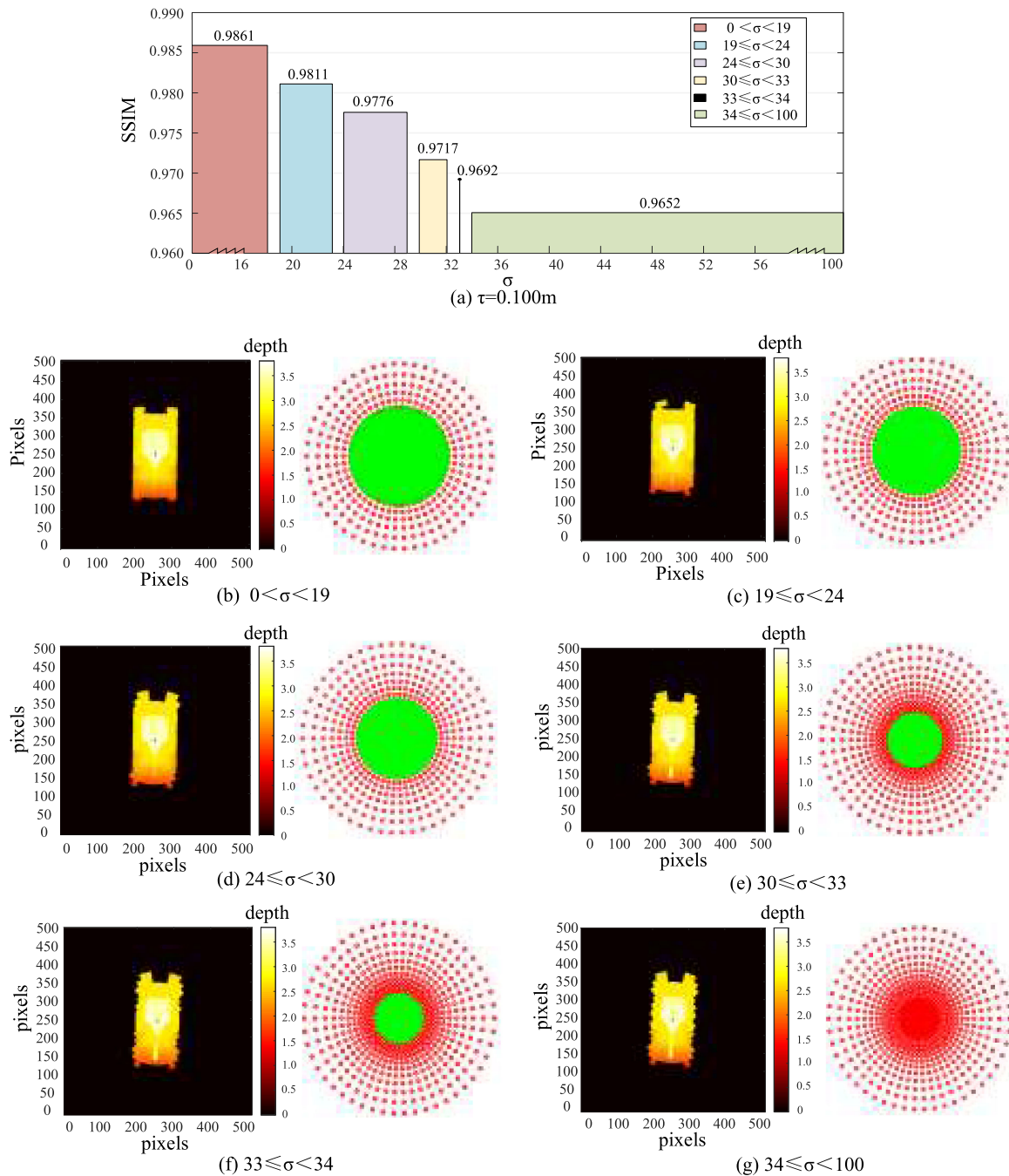


Fig. 14. (a) SSIM values in different ranges of σ ; (b)–(g) Imaging results of the target (left) and the corresponding scanning trajectory (right) in different ranges of σ .

5. Conclusion and Futureworks

In this study, a spatially adaptive retina-like sampling method for 3D laser imaging is proposed, and a mathematical model is developed. The proposed method samples the entire FOV with different decreasing coefficients, according to the depth discontinuity between the uninterested and interested objects, i.e., a large decreasing coefficient for the uninterested object and a small

decreasing coefficient for the interested object. When the proportion of the target's size and the FOV's size is 40%, the previous retina-like sampling method samples the entire FOV with same decreasing coefficient ($q_1 = 0.8818$) are compared with the proposed method samples the entire FOV with two decreasing coefficients ($q_1 = 0.8818$, $q_2 = 0.9691$). Results show that the proposed method provides a 15% reduction of the sampling points while possessing approximately the same resolution, compared with the previous method. Some simulations are conducted to compare the SSIMs and the number of the sampling points of the proposed method and the previous retina-like sampling method under different values of Γ_{TF} . Results indicate that the SSIM decreases with the increase in Γ_{TF} , and the proposed method only uses 77% and 87% times of the number of sampling points to obtain approximately the same imaging quality of the previous method, when the Γ_{TF} is 30% and 50%, respectively. However, when the Γ_{TF} increases up to 85%, the superiority of the proposed method weakens, because the number of the sampling points of the proposed method approximately equals to that of the previous method. A comparison of the two methods under a multi-object imaging scene is performed, and results demonstrate that the proposed method can improve the image quality of the interested target without consuming more data acquisition time.

This spatially adaptive retina-like imaging method is highly important for obtaining interested target images in a large FOV, whether in civil or military application. To search and identify unknown targets, the FOV should be set large, and our method can be a good guide to obtain target information efficiently with high precision in a large FOV. It should be noted that the proposed method is mostly applied to simple background with few range changes or no range changes. For scenes with complex backgrounds, the previous retina-like imaging method is more effective.

Future research should consider how to make the imaging process more autonomous. For example, 1) The current proposed method manually determines the center of the FOV and cannot independently select the gaze point. In future works, we will study how to achieve autonomy in selecting the center of the FOV and the gaze point; 2) In the proposed method, the adaptive sampling model depends on many parameters, including the number of rings and sectors, the thresholds, the radius of sampling FOV, etc. Therefore, the manner by which the optimal parameters are selected according to different applications or different scenarios is one of future research directions.

References

- [1] B. Schwarz, "Mapping the world in 3D," *Nature Photon.*, vol. 4, no. 7, pp. 429–430, 2010.
- [2] S. Jahromi, J. P. Jansson, and J. Kostamovaara, "Solid-state 3D imaging using a 1 nJ/100 ps laser diode transmitter and a single photon receiver matrix," *Opt. Exp.*, vol. 24, no. 19, pp. 21619–21632, 2016.
- [3] A. Maccarone *et al.*, "Underwater depth imaging using time-correlated single-photon counting," *Opt. Exp.*, vol. 23, no. 26, pp. 33911–33926, 2015.
- [4] M. D. Panah, B. Javidi, and E. A. Watson, "Three dimensional object recognition with photon counting imagery in the presence of noise," *Opt. Exp.*, vol. 18, no. 25, pp. 26450–26460, 2015.
- [5] M. Imaki, S. Kameyama, E. Ishimura, M. Nakaji, H. Yoshinaga, and Y. Hirano, "Line scanning time-of-flight laser sensor for intelligent transport systems, combining wide field-of-view optics of 30 deg, high scanning speed of 0.9 ms/line, and simple sensor configuration," *Opt. Eng.*, vol. 56, no. 3, 2016, Art. no. 031205.
- [6] J. Yang, L. Qiu, W. Zhao, Y. Shen, and H. Jiang, "Laser differential confocal paraboloidal vertex radius measurement," *Opt. Lett.*, vol. 39, no. 4, pp. 830–833, 2014.
- [7] C. Fu, A. Carrio, and P. Campoy, "Efficient visual odometry and mapping for unmanned aerial vehicle using ARM-based stereo vision pre-processing system," in *Proc. Int. Conf. Unmanned Aircraft Syst.*, 2015, pp. 957–962.
- [8] F. Amzajerdian *et al.*, "Recent development of 3D imaging laser sensor in Mitsubishi Electric Corporation," *Proc. SPIE*, vol. 8905, 2013, Art. no. 89052V.
- [9] H. Gao, Y. Zhang, and H. Guo, "Multihypothesis-based compressive sensing algorithm for non-scanning three-dimensional laser imaging," *IEEE J. Select. Topics Appl. Earth Observ. Remote Sens.*, vol. 11, no. 1, pp. 311–321, 2018.
- [10] R. Moss *et al.*, "Low-cost compact MEMS scanning lidar system for robotic applications," *Proc. SPIE*, vol. 8379, 2012, Art. no. 837903.
- [11] Y. Cai, X. Tong, P. Tong, H. Bu, and R. Shu, "Linear terrestrial laser scanning using array avalanche photodiodes as detectors for rapid three-dimensional imaging," *Appl. Opt.*, vol. 49, no. 34, pp. 11–19, 2010.
- [12] C. Niclass and E. Charbon, "A single photon detector array with 64×64 resolution and millimetric depth accuracy for 3D imaging," in *Proc. IEEE Int. Solid-State Circuits Conf. Digest Techn. Papers*, 2005, pp. 364–604.
- [13] C. Y. Chen, C. Li, M. Fiorentino, and S. Palermo, "A 52 ps resolution ILO-based time-to-digital converter array for LIDAR sensors," in *Proc. Circuits Syst. Conf.*, 2016, pp. 1–4.

- [14] M. Henriksson, H. Larsson, C. Grönwall, and G. Tolt, "Continuously scanning time-correlated single-photon-counting single-pixel 3-D lidar," *Opt. Eng.*, vol. 56, no. 3, 2016, Art. no. 031204.
- [15] L. Ye, G. Gu, W. He, H. Dai, J. Lin, and Q. Chen, "Adaptive target profile acquiring method for photon counting 3-d imaging lidar," *IEEE Photon. J.*, vol. 8, no. 6, Dec. 2016, Art. no. 6805510.
- [16] J. Cao *et al.*, "Design and realization of retina-like three-dimensional imaging based on a MOEMS mirror," *Opt. Lasers Eng.*, vol. 82, pp. 1–13, 2016.
- [17] J. Cao *et al.*, "Modeling and simulations of three-dimensional laser imaging based on space-variant structure," *Opt. Laser Technol.*, vol. 78, pp. 62–70, 2016.
- [18] P. Shilane, P. Min, M. Kazhdan, and T. Funkhouser, "The Princeton Shape Benchmark," Shape Modeling International, Genova, Italy, Jun. 2004. [Online]. Available: <http://shape.cs.princeton.edu/benchmark/>
- [19] Z. Wang, A. C. Bovik, H. R. Sheikh, and E. P. Simoncelli, "Image quality assessment: From error visibility to structural similarity," *IEEE Trans. Image Process.*, vol. 13, no. 4, pp. 600–612, Apr. 2004.
- [20] Q. Yuan, L. Zhang, and H. Shen, "Regional spatially adaptive total variation super-resolution with spatial information filtering and clustering," *IEEE Trans Image Process*, vol. 22, no. 6, pp. 2327–2342, Jun. 2013.
- [21] Q. Hao, Y. Xiao, C. Jie, C. Yang, and C. Sun, "Improving the performances of autofocus based on adaptive retina-like sampling model," *Opt. Commun.*, vol. 410, pp. 269–276, 2018.
- [22] I. Lee, M. T. Mahmood, and T. S. Choi, "Adaptive window selection for 3D shape recovery from image focus," *Opt. Laser Technol.*, vol. 45, no. 1, pp. 21–31, 2013.